*Journal of The Electrochemical Society*, **161** (3) F354-F359 (2014)
0013-4651/2014/161(3)/F354/6/$31.00 © The Electrochemical Society

# A Fuel-Flexible Solid Oxide Fuel Cell Operating in Gradual Internal Reforming

**Shayenne D. Nobrega,[a,c] Patrick Gelin,[b] Samuel Georges,[c] Marlu C. Steil,[c] Bruno L. Augusto,[d] Fabio B. Noronha,[d] and Fabio C. Fonseca[a,*,z]**

[a]*Instituto de Pesquisas Energéticas e Nucleares, IPEN, São Paulo, SP 05508-000, Brazil*
[b]*Université Lyon 1, CNRS, UMR 5256, IRCELYON, Institut de recherches sur la catalyse et l' environnement de Lyon, F-69626 Villeurbanne, France*
[c]*Laboratoire d'Electrochimie et de Physicochimie des Matériaux et des Interfaces, UMR 5279, CNRS-Grenoble INP-UJF - BP75, 38402 Saint Martin d'Hères, France*
[d]*Instituto Nacional de Tecnologia, INT,, Rio de Janeiro, RJ 20081-312, Brazil*

An electrolyte supported solid oxide fuel cell (SOFC) was continuously operated with hydrogen, methane, and bioethanol for nearly 400 hours without adding water, $O_2$, or $CO_2$, and delivering a rather stable power output. Such a fuel-flexible SOFC was achieved by using both an anodic catalytic layer, which efficiently converts the primary fuel into hydrogen, and by the operation in gradual internal reforming conditions, which prevented degradation due to carbon formation.
 [DOI: 10.1149/2.107403jes] 

Manuscript submitted October 24, 2013; revised manuscript received January 9, 2014. Published January 17, 2014.

Fuel cell development is driven by the urgent need of high efficiency and less environmental impact for the increasing demand of energy supply. Solid oxide fuel cells (SOFCs) are potentially the most efficient technology to convert chemical energy into electricity and thus could have a major impact on reducing fuel consumption and $CO_2$ emissions.[1,2] The high operating temperature, typically ≥600°C, confer SOFCs the potential to run on both conventional fuels (e.g., natural gas, gasoline, and diesel) and biofuels (e.g., biogas, ethanol, and biodiesel). Such unique fuel flexibility and unsolved problems concerning both the production and the storage of hydrogen have encouraged a great number of studies on SOFCs operating with alternative fuels.[3–9] However, several practical issues have prevented a more widespread use of fuels other than hydrogen. The catastrophic degradation of the standard Ni-based cermet anodes when carbon containing fuels are fed to the fuel cell is a major hurdle. Thus, effective demonstrations of fuel flexible SOFCs by showing long term operation using different fuels with performance comparable to hydrogen are rarely found.

Methane is possibly the most studied alternative fuel for SOFCs because it is abundant and the main constituent of both natural and biogas. Nonetheless, most of the reported substitutes for hydrogen have been non-renewable fuels.[3–6] One of the few notable exceptions is bioethanol.[7–9] Sugar cane derived ethanol is a cost competitive and efficient biofuel that has received increasing attention.[7,10,11] Ethanol is a liquid fuel that has high energy density that can be easily stored and transported, and has great potential for hydrogen production with high efficiencies and zero net carbon emission.[10] As compared to other renewables such as biodiesel and biogas, ethanol exhibits two important characteristics for SOFCs: fixed composition and insignificant sulfur contamination.

In this context, the development of fuel-flexible anodes could disconnect SOFCs from the (still to come) hydrogen infrastructure and would greatly push this technology toward commercialization. Indeed, SOFC operation on biofuels is the most energy efficient means to utilize home grown carbon neutral fuels.[2,10]

However, due to the limitations of the standard Ni cermets, stable operation of SOFCs running on both hydrocarbons and alcohols requires the development of specific anode designs. Alternative anodes aiming at the direct oxidation of primary fuels have been demonstrated, showing reasonable stability in short term tests, but usually resulting in significantly lower performance than the Ni cermet running on hydrogen.[3] In fact, no substitute for the Ni cermet has been found to combine simple processing, stability, and good catalytic and electrochemical properties, as demanded by high-performance SOFC.[3] Conversely, using Ni cermets for the internal reforming in SOFCs requires large amounts of water (or other reforming gas) to prevent carbon formation, decreasing efficiency and increasing system complexity.[3,4,12,13]

An interesting approach has been the decoupling of the catalytic and electrochemical functions of the anode by adding an active layer to process the fuel and protect the anode.[4,12] By using such a catalytic layer some studies have demonstrated SOFCs running on carbon containing fuels with satisfactory performance and stability; however, most of those studies add an oxidizing agent, usually water, to the fuel to ensure the stability of the anode.[3,4,12–14] Alternatively, the gradual internal reforming (GIR)[15] was theoretically[16,17] and experimentally demonstrated to result in long-term stability of SOFCs operating without added water.[18–21] In the GIR, the water released by the electrochemical oxidation of hydrogen at the anode is used for the steam reforming of the fuel in the catalytic layer deposited over the anode. A scheme of GIR unit cell and reactions on the direct conversion of methane and ethanol are shown in Figure 1. The unit cell is comprised of a lanthanum manganite (LSM) cathode, YSZ (yttria-stabilized zirconia) electrolyte, Ni/YSZ anode, and an iridium / gadolinia-doped ceria (Ir/CGO) catalytic layer. Ceria-based oxides are convenient and compatible materials for SOFCs.[22] Thus, as long as the fuel cell is polarized, producing water, both the catalytic and electrochemical reactions sustain each other and the primary fuel is gradually consumed, avoiding thermal stress due to rapid endothermic reforming reactions.

In the present study, the role of the catalytic layer for the stable operation of the fuel cell running on different fuels was investigated. In the first part the catalytic properties of Ir/CGO for ethanol conversion were studied and in the second part it was demonstrated that a suitable catalytic layer allows for the fuel flexibility in SOFC.

## Experimental

*Fabrication and characterization of Ir/CGO catalyst.*— The catalytic layer of $Ce_{0.9}Gd_{0.1}O_{2-x}$ (CGO, Praxair) containing 0.1 wt% of Ir (Ir/CGO) was prepared by an impregnation technique.[23] The appropriate amount of iridium acetylacetonate (Alfa Aesar) solution in toluene was added to a suspension of CGO. After evaporation of the solvent under reduced pressure, the catalyst was calcined in flowing $O_2$ at 350°C for 6 h.

The catalytic study of steam reforming (SR) of ethanol was performed in a quartz reactor at atmospheric pressure. A small amount of catalyst (20 mg) was used in order to study the catalyst deactivation within a short period of time. The samples were diluted with inert SiC (SiC mass/catalyst mass of 3.0). Before the catalytic tests, the samples were reduced in situ under $H_2$ at 500°C for 1 h and then purged under $N_2$ at the same temperature for 30 min. All reactions

*Electrochemical Society Active Member.
[z]E-mail: fcfonseca@ipen.br

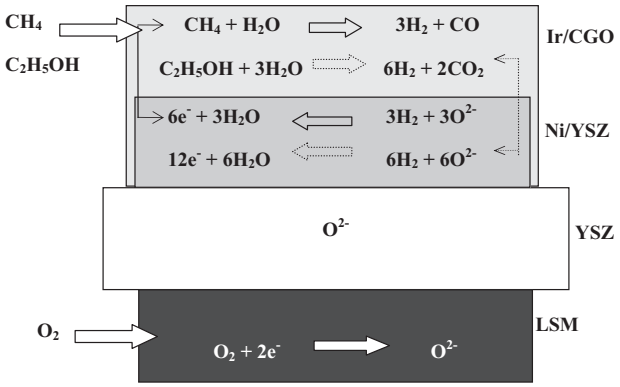


**Figure 1.** Scheme of gradual internal reforming unit cell and reactions for the direct conversion of methane and ethanol. The unit cell is comprised of a lanthanum manganite (LSM) cathode, YSZ (yttria-stabilized zirconia) electrolyte, Ni/YSZ anode, and Ir/CGO (gadolinia-doped ceria) catalytic layer.

were performed at 850°C using an $H_2O$/ethanol molar ratio of 3.0. The reactant mixture (2.5% ethanol; 7.5% water, 90.0% nitrogen) was obtained by flowing two $N_2$ streams (30 mL/min) through each saturator containing ethanol and water separately.

Temperature-programmed oxidation experiments ($O_2$-TPO) were performed using a Pfeiffer Omnistar Quadrupole Mass Spectrometer (QMS) after catalytic tests. After testing, samples were exposed in air. 20 mg of each sample (mixture of catalyst and SiC in 1:3 ratio) were introduced in a U-shaped quartz reactor and deposited on a quartz wool plug. The sample was exposed to a 0.5 vol% $O_2$/0.5 vol% Ar/99 vol% He flow (1.8 L $h^{-1}$) at room temperature and the temperature was linearly increased from room temperature up to 900°C at the rate of 10 °C $min^{-1}$ and held at 900 °C for 15 min. $O_2$ (m/e = 32), CO (m/e = 28) and $CO_2$ (m/e = 44) were continuously monitored. The signal m/e = 28 was corrected for the contribution of the $CO_2$ fragmentation in order to obtain the CO concentration. Calibrations were performed using 1% CO/He, 1% $CO_2$/He and 1% Ar/He mixtures (Air Liquide).

*Fabrication and tests of solid oxide fuel cells.*— Electrolyte supported cells were fabricated using yttria-stabilized zirconia (YSZ) substrates (56 mm diameter and ∼1 mm thick). Electrode layers were deposited by spin coating: (a) $La_{0.65}Sr_{0.30}MnO_3$ (LSM) and LSM/YSZ (50/50 wt%) for current collector and functional cathode layers, respectively; (b) Ni/YSZ 60/40 vol% and 40/60 vol% for current collector and functional anode layers, respectively; and (c) Ir/$Ce_{0.9}Gd_{0.1}O_{2-x}$ catalytic layer.

The YSZ (8 mol% yttria, Tosoh) electrolyte was produced by uniaxial and isostatic pressing (2500 bar) followed by sintering at 1450°C for 2 h. The LSM cathode was synthesized by the polymeric precursor technique using high-purity (> 99%) nitrates (Aldrich) as starting materials,[24] followed by calcination at 800°C for 3 h. Composites Ni/YSZ were prepared by a liquid mixture technique[25] using a solution of nickel acetate (Aldrich) in ethanol, evaporated at 70°C and calcined at 450°C for 5 h. Suspensions for spin-coating deposition were prepared by mixing terpineol (56.5 wt%), ethylcellulose (3.5 wt%), and the respective powder of each electrode layer (40 wt%), followed by homogenization by ball milling with yttria-stabilized (3 mol%) zirconia grinding media for 15 h. The spin-coating depositions were carried out at 6000 rpm for 5 s followed by drying in a hot plate (80°C for 5 min). Anode and cathode were sintered at 1400°C and 1150°C for 1 h, respectively. Total thickness of anode and cathode layers were ∼60 μm and 80 μm, respectively, each having a ∼20 μm thick functional layer. The active electrode area was 13.8 $cm^2$.

The Ir/CGO catalytic layer was deposited onto the anode by spray-coating of ethanol/terpineol-based suspension with organic additives. After the coating step the catalytic layer was heated at 900°C for 2 h in flowing argon. The amount of catalyst deposited was 0.8 g, corresponding to a final thickness of the catalytic layer of ∼ 80 μm. The amount of Ir (∼0.04 mg $cm^{-2}$) is one order of magnitude lower than the state-of-the-art Pt loading in polymer membrane fuel cells.

The single cell was set up between two alumina tubes (anode and cathode side) using gold rings for the sealing, as reported elsewhere.[19,20] Alumina capillaries were inserted in the concentric tubes for both gas delivery and electric terminals. Gold wires allow independent measurements of the current and the potential in a 4-wire configuration. The system is closed with a metallic head sealed with rubber gaskets. Fuel cell tests were performed at 850°C with flowing synthetic air in the cathode side (5 L $h^{-1}$). Fuel cells were initially operated on $H_2$ (60%) and after anode reduction and stable OCV = 1.12 V, the electrochemical properties were studied under hydrogen, ethanol, and methane, without water addition. Hydrogen (60%) was switched to the desired fuel: methane (20%) or ethanol (10%). As previously demonstrated,[19,20] such fuel concentrations were used to keep the theoretical number of electrons constant (as calculated from the reactions in Figure 1) for each fuel and to keep constant the steam release required for the catalytic fuel conversion in the Ir/GCO layer. Fuels were carried by argon at total flow rate of 4 L $h^{-1}$ set by calibrated mass flowmeters (Brooks Instr.). Liquid ethanol was kept in a thermal bath with controlled temperature of 29°C. The fuel cell was continuously operated for ∼390 hours during which the three fuels were repeatedly changed. Electrochemical impedance spectroscopy (EIS) and polarization vs. time (i-*t*) measurements were performed by an Autolab PGSTAT128N potentiostat with a BSTR10A current booster. A variable resistor bench connected in series with the fuel cell was used for polarization curve (V-i) measurements. For each measured cell potential the system was allowed to stabilize for 0.5 h before recording the electrical current.

Scanning electron microscopy analyzes of the fractured surface of the anode were carried out after the fuel cell operation.

## Results and Discussion

*Catalytic properties of Ir/CGO.*— In this study, the reliable and fuel-flexible operation in ethanol and methane requires a detailed characterization of the catalytic properties of the Ir/CGO layer in both fuels. Previous reports have shown that the Ir/CGO was stable for the internal reforming of methane.[19,20,26,27] Thus, such catalyst was studied in detail for the ethanol steam reforming (SR). Ethanol conversion and product distributions as a function of time-on-stream (TOS) for SR of ethanol, with $H_2O$/ethanol molar ratio of 3.0, over CGO and Ir/CGO catalysts are shown in Figure 2. For CGO sample, ethanol conversion remained constant at around 100% during 25 h TOS. The main products formed were $H_2$, CO, $CH_4$, and $CO_2$. However, the selectivity to $H_2$ decreased whereas the formation of ethylene and methane increased during the reaction, possibly indicating some deactivation of the CGO catalyst with TOS. For Ir/CGO catalyst, the complete ethanol conversion was also achieved during 25 h TOS. However, there are significant differences in the products distribution. The addition of Ir decreased the production of methane and increased the formation of $H_2$. Furthermore, the formation of ethylene was inhibited and, contrary to CGO, no change in the products distribution was observed during 25 hours of TOS.

According to the reaction mechanism for SR,[28] ethanol may be dehydrogenated to acetaldehyde or dehydrated to ethylene. Acetaldehyde may be further dehydrogenated and oxidized to acetate species that can either decompose to $CH_4$ and CO or produce carbonate species. Ethylene can undergo further reactions such as oligomerization, aromatization, or cracking, producing benzene, toluene, or xylenes (BTX). Such reactions may be responsible for coke formation and catalyst deactivation. Comparing products distributions obtained with the two catalysts at early stages of the catalytic testing suggests that Ir addition to CGO enhances the ethanol dehydrogenation rate, as usually observed over noble metals catalysts, and promotes the steam reforming of methane thus produced. It has been previously reported that doping CGO with traces of Ir improves the rate of methane steam reforming by more than two orders of magnitude compared to the rate

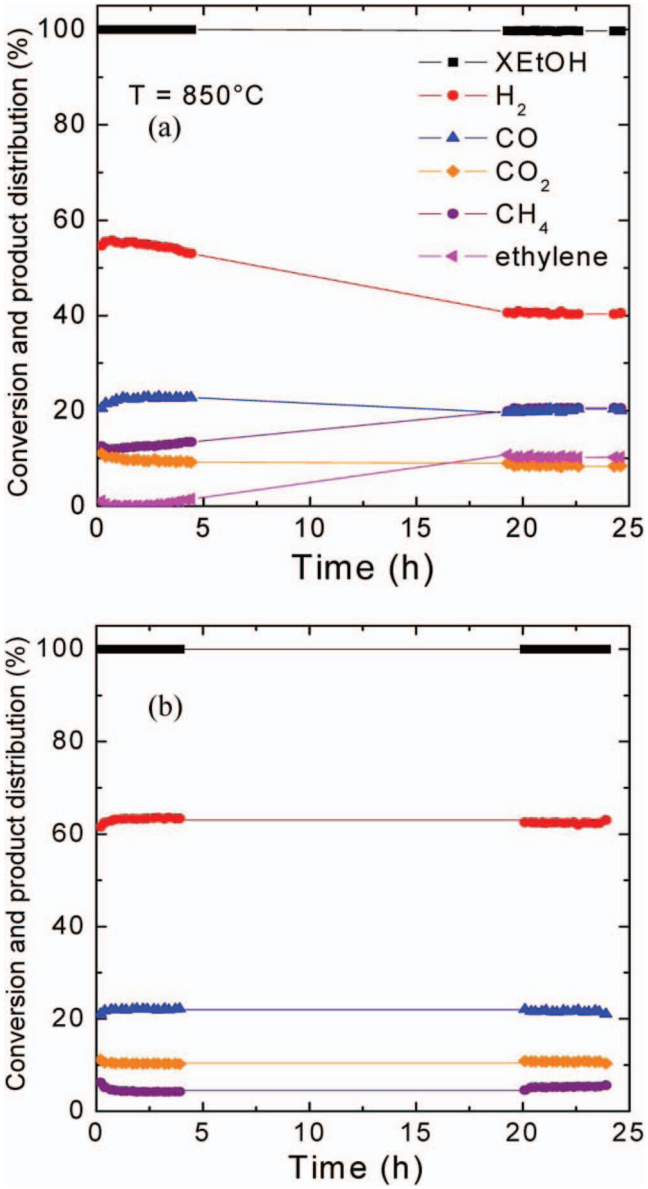


**Figure 2.** Ethanol conversion (X EtOH) and product distribution as a function of time-on-stream for (a) CGO and (b) Ir/CGO.

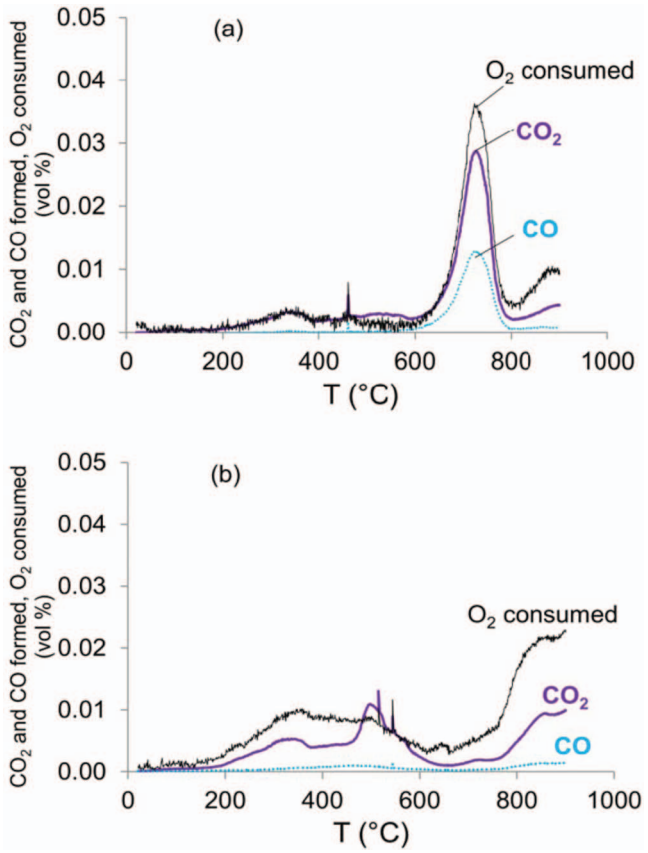


**Figure 3.** Profiles of $CO_2$, CO formation and $O_2$ consumption during $O_2$-TPO over CGO (a) and Ir/CGO (b) after catalytic testing.

obtained with undoped CGO.[26,27] However, it is important to consider that ethanol can undergo decomposition in the gas phase at 850°C.[29] This could occur to some extent in the hot section of the reactor before ethanol reaches the catalyst bed heated at 850°C. According to a kinetic model,[29] predicted major species formed by ethanol pyrolysis at 800°C were, by decreasing order of concentrations, $H_2O$, $C_2H_4$, $H_2$, CO and $CH_4$. We have experimentally observed the same products when feeding the reactor containing only the quartz wool plug (no catalyst) with a 2.5 vol% EtOH / 97.5 vol% $N_2$ mixture at 850°C, except the order was different: $H_2$ (34%), CO (28%), $CH_4$ (23%), and ethylene (15%). Interestingly, the molar composition of products ($H_2O$ being excluded) obtained in the ethanol decomposition was close to that obtained after 25 h TOS over the CGO catalyst bed. This is a further indication that CGO was mostly deactivated after 25 h reaction with $EtOH/H_2O/N_2$ mixture and that essentially homogenous pyrolysis of ethanol proceeded at this stage. Homogenous steam reforming can be ruled out in such conditions.[29] The formation of carbon deposits possibly responsible for CGO deactivation was therefore expected and further confirmed by TPO of the sample after testing (pl., see Fig. 3). If it is clear that the homogenous pyrolysis pathway might proceed in the absence of catalyst or over fully deactivated catalyst, the estimate of this pathway compared to the catalytic steam reforming of ethanol over active catalyst is not possible. It may be anticipated that it is strongly dependent on the residence time of the reactants in the hot zone before the catalytic bed, which is very small in our experiments (volume of the hot zone above the catalyst $<1$ cm$^3$, residence time $<1$ s). The main point is that irrespective of the real composition of the reaction mixture being in contact with the Ir/CGO bed, $H_2$, CO, and $CO_2$ are the main products while ethylene is not detected and $CH_4$ concentration is low. This supports the idea that Ir/CGO is suitable for the application, being active in the catalytic conversions of these two undesired products (partially for $CH_4$ and totally for $C_2H_4$) either being formed by catalytic steam reforming or homogeneous pyrolisis of ethanol.

After catalytic tests, CGO and Ir/CGO samples were analyzed by TPO experiments. Profiles of CO and $CO_2$ along with consumed $O_2$ versus temperature, corresponding to CGO and Ir/CGO, are shown in Figure 3. For both samples, below 600°C broad, ill-defined, and small peaks of $CO_2$ formation can be distinguished while $O_2$ is being consumed and no CO is produced. Such feature indicates that some carbon species have been formed during catalytic testing and are fully oxidized to $CO_2$. For CGO, at least two types of carbon species (peaks occurring at ~350 and 550°C) could be identified. The $O_2$ consumption and the $CO_2$ release are in good agreement, being 208 μmol/g catalyst.

For Ir/CGO, two main peaks of $CO_2$ formed can be identified at ~330 and 500°C, suggesting at least two different types of C species being fully oxidized. It can be remarked that the amount of $O_2$ consumed below 450°C significantly exceeds that of $CO_2$ release while the reverse is observed above 450°C. Such a behavior suggests the transient formation of stable carbonates below 450°C, which are decomposed above such temperature. The amount of $CO_2$ released

below 600°C was 416 μmol/g catalyst. Above 600°C a sharp peak corresponding to the simultaneous formation of $CO_2$ and, to a lower extent, CO is observed at ~720°C for the CGO sample, while for the Ir/CGO sample such a peak is absent. The amount of released $CO_2$ (596 μmol/g catalyst) and CO (272 μmol/g catalyst) is fully consistent with the amount of consumed $O_2$ according to the stoichiometry of corresponding C oxidation reactions. This peak is attributed to the oxidation of graphitic carbon (868 μmol/g sample). Above 800°C, increasing amounts of $CO_2$ start to form while twice as much $O_2$ amounts are consumed simultaneously. This feature is attributed to the slow oxidation of small amounts of SiC.[30]

Based on the $O_2$-TPO data, it is possible to observe that both CGO and Ir/CGO allow the formation of limited amounts of carbon species (respectively 1076 and 416 μmol/g sample) during catalytic testing on ethanol. Moreover, TPO data clearly indicate that graphitic carbon forms only in the CGO sample and that Ir addition to the catalyst hinders such a carbon. Both the higher resistance of Ir/CGO to carbon formation and its inhibiting effect to the accumulation of graphitic forms are directly related to the product distribution of this sample during steam reforming of ethanol at 850°C. For CGO, the resistance to carbon formation is lower, which leads to catalyst deactivation. Based on the promising catalytic activity Ir/CGO has been proposed for the reforming of ethanol and methane. Therefore, such catalysts were deposited onto the anode of single cells for testing the operation under methane and ethanol.

*Solid oxide fuel cell tests.*— The electrochemical properties of fuel cells with the Ir/CGO catalytic layer were studied during operation on $H_2$/Ar (60/40%), $CH_4$/Ar (20/80%), and $C_2H_5OH$/Ar (10/90%). Polarization curves were firstly measured under hydrogen at 850°C. After polarization measurements the fuel cell was kept at 0.8 V under $H_2$ and the fuel was switched to methane, and the system was stabilized for 0.5 h. The same procedure was used when the fuel was changed from methane to ethanol. Figure 4 shows polarization (V-*i*) curves for the fuel cell operating on different fuels.

Under $H_2$ the polarization curves were recorded from OCV to 0.4 V, whereas for the other fuels maximum cell voltage was 0.8 V because GIR requires that the fuel cell is kept under polarization to sustain the reactions depicted in Figure 1. The V-*i* curves taken under $H_2$ exhibited a small activation polarization at low current densities *i*. With increasing *i* a rather linear behavior is observed, which is associated with the ohmic losses. The maximum power density ~100 mW $cm^2$ at 0.5 V was limited mostly by the thick supporting electrolyte.

The polarization curves on both methane and ethanol are rather linear in the *i* range measured, similarly to that on hydrogen. In fact, the V-*i* curves showed comparable performances under the different fuels. Such a feature is markedly different from usually reported results

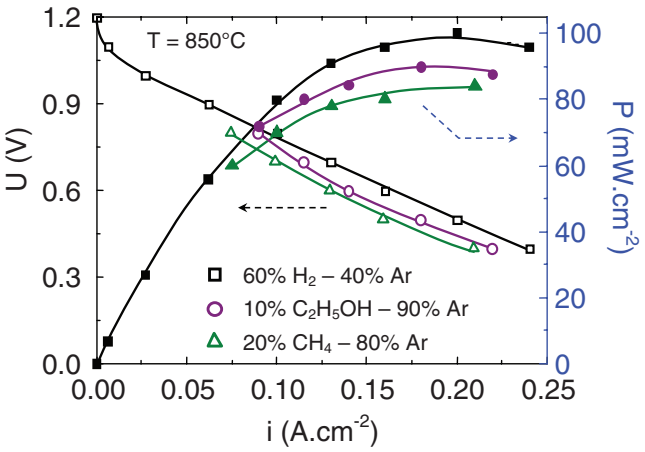


**Figure 4.** Polarization curves measured at 850°C for hydrogen, ethanol, and methane.

in which significant performance drop is observed when hydrogen is substituted by other fuels.[31,32] It is also important to consider that both methane and ethanol concentration were adjusted with respect to hydrogen in order to keep the theoretical number of electrons constant —thus the resulting current density— according to the equations in Figure 1. Such features were previously discussed in detail in Refs. 19 and 20. Besides, the dilution of the fuel decreases the fuel cell performance.[20] Nevertheless, a decrease of ~20% of the maximum power output is observed, a feature more evident for methane. Such a performance drop is possibly related to a decreased faradaic efficiency when larger fuel molecules are firstly converted to hydrogen in the catalytic layer prior to the electrochemical oxidation at the anode/electrolyte triple phase boundary. It should be considered that the electrolyte supported fuel cell configuration, with relatively thin anode, may eventually hinder some adverse effects due to the catalytic layer that could be more pronounced in anode supported fuel cells. In this scenario, parameters such as the thickness and porosity of the catalytic layer are likely to play an important role for the fuel cell performance. The microstructure of the anode/catalytic layer interface must be optimized to allow an easy access of both the fuel and the steam released by the anode to the catalytic sites along with a low impedance transport of hydrogen to the anode triple phase boundaries. Nonetheless, the relatively small differences on the polarization curves indicate that the GIR model depicted in the Figure 1 is reasonable, but may not fully represent all possible reaction paths for each fuel. A relevant point is that ethanol decomposes at the operating temperature (850°C); nevertheless, decomposition products are likely to result in coke formation if inadequate catalysts are used. Even though water is the main product of ethanol decomposition,[29] dry ethanol cannot be fed to the conventional Ni-based cermet anode without severe degradation after few hours of operation. A possible issue is the reactivity of ethylene, which is the coke precursor and is inhibited when using Ir/CGO catalyst. Thus, the results in Figure 4 suggest that the Ir/CGO layer is an effective catalyst for the gradual internal reforming of both methane and ethanol. Such a feature was further studied by stability tests of the fuel cell operating on different fuels.

Assuming a faradaïc efficiency of 1 for the electrochemical oxidation of $H_2$, the fuel utilization ($U_f$) was adjusted for the stability tests.[20,21] According to the model describing both the catalytic and the electrochemical reactions shown in Figure 1, a minimum $U_f$ must be achieved to ensure enough steam release from the anode for the complete conversion of the fuel in the catalyst layer. In the case of methane and ethanol, the stoichiometry indicates a critical fuel utilization of 1/3 and 1/2, respectively. Below such theoretical limit the fuel cell produces insufficient steam to ensure the complete conversion of the fuel, resulting in fuel diffusion into the Ni/YSZ cermet and possible carbon deposition. Figure 5 shows the dependence of the fuel utilization on different operating voltages for the three studied fuels. In the present study, the output voltage (0.6 V) was selected to ensure fuel utilizations close to the critical values for both methane and ethanol. In the case of ethanol, the ratio 1/6 to hydrogen, to keep the theoretical number of electrons constant, prevented the increase of the fuel concentration and $U_f$ was set at ~35%. Such a value is below the stoichiometric value for complete steam reforming of ethanol and indicates that other reaction take place, possibly due to ethanol decomposition before reaching the catalytic layer.[29]

Figure 6 shows the time (*t*) dependence of *i* (at 0.6 V) using $H_2$, methane, and ethanol. The operation was initiated in $H_2$ and after a steady operation (~1 h) fuel was changed to methane and ethanol.

The most important result shown in Figure 6 is the good stability of the fuel cell operating on three distinct fuels without water addition for a long time period (~400 h). After initial operation on $H_2$ (~1 h), the fuel cell quickly stabilized under methane, with $i \sim 0.12$ A $cm^{-2}$. The current density showed some variations depending on the fuel, in agreement with the polarization curves (Figure 4). After ~10 h on methane, the fuel was switched to ethanol, in which a stable $i \sim 0.125$ A $cm^{-2}$ was recorded for ~100 h. After ~150 hours of continuous operation, the fuel was switched again to $H_2$ and $i \sim 0.135$ A $cm^{-2}$ was monitored for ~50 h. The fuel flexibility was further tested

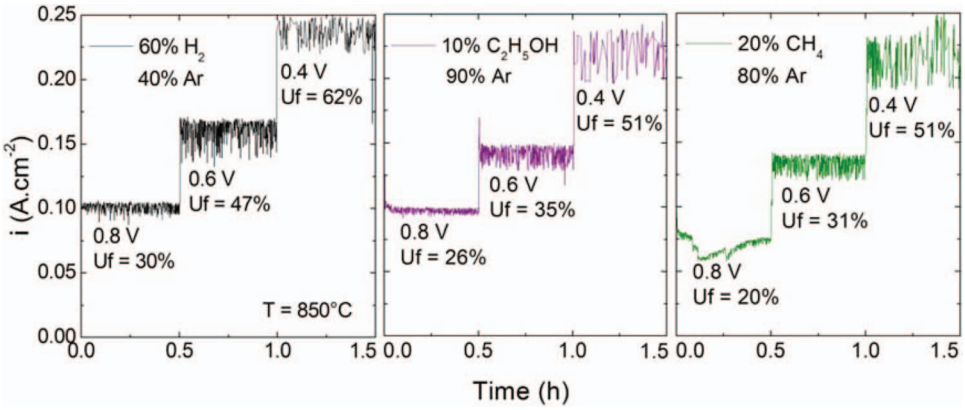


**Figure 5.** Fuel utilization for hydrogen, ethanol, and methane under polarization of 0.8 V, 0.6 V, and 0.4 V.

by changing again the fuel from $H_2$ to methane. From $t = 160$ h up to 240 h the fuel cell operating on methane exhibited slight decay from $i = 0.110$ A cm$^{-2}$ to 0.105 A cm$^{-2}$. Nevertheless, it is interesting to note that upon switching the fuel back to hydrogen the fuel cell essentially recovers the previous measured i ~0.135 A cm$^{-2}$. Finally, hydrogen was changed to ethanol and once again and a rather stable $i$ ~0.115 A cm$^{-2}$ was measured for more than 100 hours. The current density at 0.6 V exhibited a total decay of ~5% in 390 h of operation. This is a relatively high degradation rate when compared to the state-of-the-art fuel cells, but it is markedly lower than degradation resulting from carbon formation.[33] The results shown in Figs. 4 and 6 are a strong indication that the catalytic layer protects the anode and prevents carbon deposition, which would result in fast and pronounced current drop. In addition, the experimental data demonstrate an efficient conversion of both methane and ethanol in the catalytic layer. The similar $i$ output measured for methane and ethanol suggests that hydrogen is the effective fuel, as described by the ideal GIR mechanisms represented in Figure 1.

It is interesting to note that a stable operation was obtained with fuel utilization lower than the critical value for ethanol. Such a feature indicates that additional conversion mechanisms to those depicted in Figure 1 may occur in the system. Indeed, the catalytic tests (Figure 2b) showed that the conversion of ethanol over Ir/CGO yields the formation of $H_2/CH_4$ mixture (60% / 5%). By considering such a ratio it is possible to calculate that fuel concentration is ~75%, which corresponds to the theoretical stoichiometry indicated for the steam reforming of ethanol in Figure 1. Moreover, ethanol pyrolysis may occur upstream the fuel cell. Thus, in the case of ethanol, the species available for catalytic conversion within the active layer may be different than the fuel being fed to the cell. Previous studies showed that ethanol is completely decomposed above 800°C with a residence time of ~4 s.[29] In the single cell test apparatus the estimated residence time at 850°C is ~25 s. This residence time is considerably larger than the one in the catalytic test setup and indicates that the pyrolysis products of ethanol are likely to be present in the catalytic layer. Ethanol pyrolysis produces relatively large amounts of water, $H_2$, CO, and $CH_4$. Nevertheless, in both cases, pyrolysis or steam reforming, the available species are either oxidized in the anode —$H_2$— or reacted with available water in the Ir/CGO layer —$CH_4$ from pyrolysis or EtOH— to produce $H_2$,[19,20,26,27] resulting in a stable operation of the fuel cell. Nonetheless, additional experiments are underway to further investigate the reactions taking place in the anode.

To further understand the operation of the fuel-flexible SOFCs and possible degradation mechanisms both impedance measurements and microstructural analyzes were carried out. Figure 7 shows impedance data taken during the stability tests both under polarization (7a) and at OCV (7b). The Figure 7a shows impedance data under 0.6 V

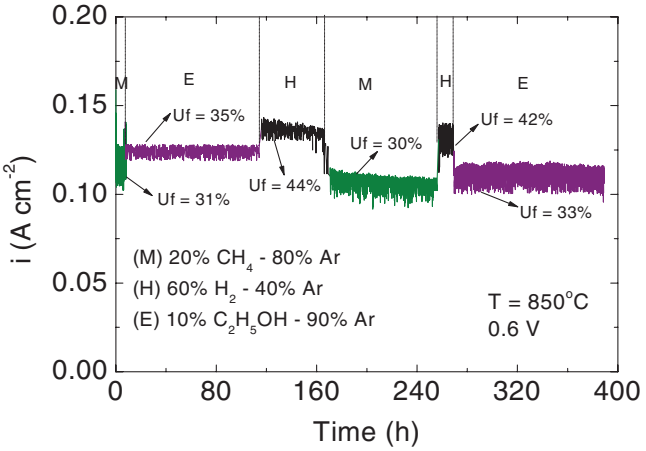


**Figure 6.** Potentiostatic test recorded at 0.6 V of single SOFC containing a ceria-based catalytic layer under hydrogen, ethanol, and methane.

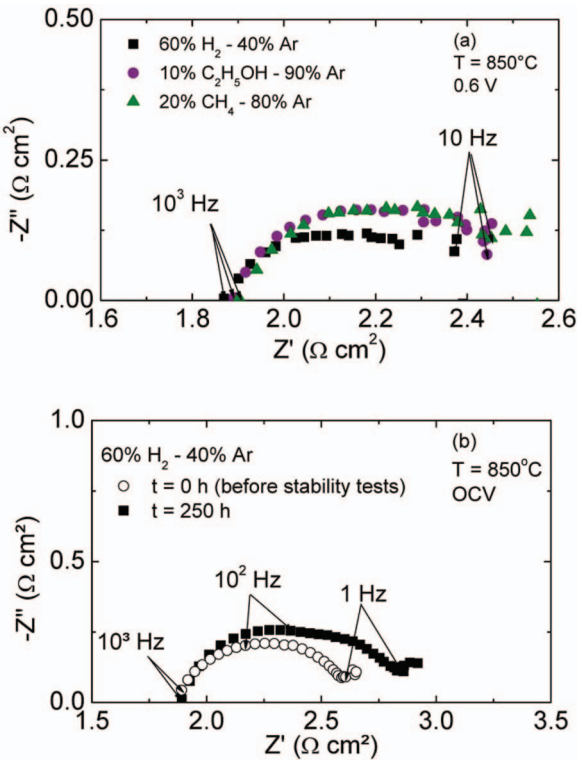


**Figure 7.** (a) Impedance measurements at 0.6 V for the fuel cell operating in hydrogen, ethanol, and methane taken during the stability tests. (b) Impedance measurements at OCV for the fuel cell operating in hydrogen before the stability test and after 250 hours of operation.

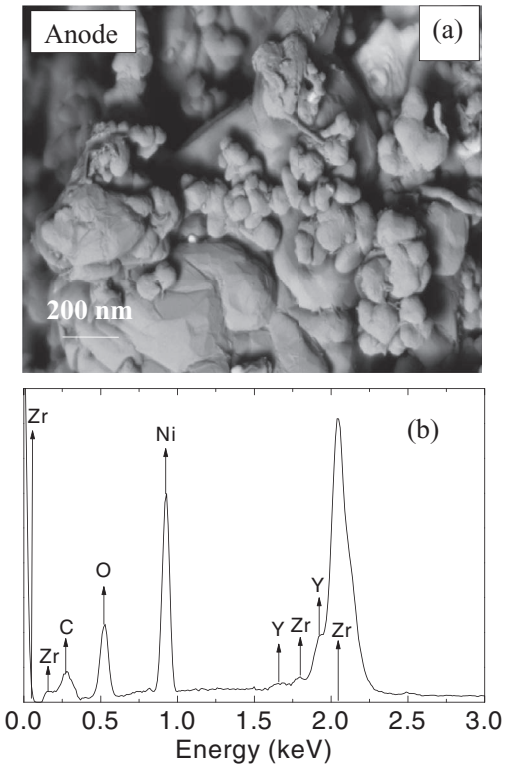


**Figure 8.** (a) Scanning electron microscopy and (b) energy-dispersive X-ray spectroscopy of the anode after 390 h of operation under hydrogen, ethanol, and methane.

polarization collected for methane, hydrogen and ethanol at $t \sim 240$, 280, and 360 h, respectively. The impedance diagrams consist of a depressed semicircle arc, and the polarization resistance reflected the variation of $i$ for each fuel (Figure 6). As compared to hydrogen, both methane and ethanol exhibited increased total resistance, mostly due to increased electrode polarization. Such results are in agreement with the polarization curves (Figure 6) that evidenced slightly increased losses for both methane and ethanol. Such losses are probably related to the complex reactions and mass transport processes taking place at both the catalytic and anodic layers when methane or ethanol are fed to the fuel cell.

Figure 7b shows the impedance data recorded under hydrogen at OCV measured before the stability tests and after ~250 hours of operation. The high frequency intercept indicates that the ohmic contribution was practically unchanged during the stability test. The non-ohmic component is composed of at least two polarization contributions in the 1 kHz–1 Hz frequency range. A visual inspection of the diagram revealed that the low frequency part showed a slight increase after 250 hours of operation at 0.6 V.

The low frequency (<1 Hz) spike is possibly related to an additional diffusion resistance due to the catalytic layer. Further studies varying the catalytic layer thickness and porosity are underway to better understand the impedance response of fuel cells with such a layer. Nonetheless, the increased polarization resistance after 250 hours of operation could not be associated to anode degradation due to carbon formation. The observed increase of the electrode polarization is likely to be due to a global degradation effect of the electrochemical properties of the fuel cell, which was not optimized for long term operation.

To investigate possible degradation due to carbon deposition on the anode, the fuel cell was analyzed by SEM and EDX after ~400 h of operation. The micrograph shown in the Figure 8a revealed well-defined and sub-micrometric grains of the Ni-cermet with a smooth microstructure, showing no evidence of carbon deposits. Usually, carbon deposition observed over Ni particles is severe and can be easily identified.[34] The corresponding EDX spectrum of the SEM image is shown in the Figure 8b. The EDX spectrum exhibits the expected peaks corresponding to Zr, Y, Ni, O, and a minor contribution corresponding to carbon could be identified. Apparently, such minor carbon formation corresponds to non-graphitic carbon as indicated in the Ir/CGO catalytic tests. Such carbon species are easily oxidized and in principle represent no major harm to the GIR.

## Conclusions

A fuel-flexible solid oxide fuel cell was demonstrated to operate on methane, bioethanol, and hydrogen for almost 400 hours without water addition and delivering similar current outputs in different fuels. The Ir/CGO catalyst allowed for stable current outputs in different fuels, indicating that the gradual internal reforming was efficient. The addition of Ir to the CGO prevented deleterious carbon formation, as inferred from both catalytic tests and the analysis of the anode microstructure after fuel cell stability tests. Based on the present results, the design of both optimized fuel cells and catalysts open the way to the development of high-performance fuel-flexible SOFCs running directly on renewable fuels.

## Acknowledgment

Thanks are due to Brazilian (CAPES, CNPq, CNEN) and French (COFECUB, ADEME) agencies for partial funding and scholarships.

## References

1. S. C. Singhal and K. Kendall, High Temperature and Solid Oxide Fuel Cells – Fundamentals, Design and Applications, p. 1 (2003).
2. E. D. Wachsman, C. A. Marlowe, and K. T. Lee, *Energ. Environ., Sci.*, **5**, 5498 (2012).
3. A. Atkinson, S. Barnett, R. J. Gorte, J. T. S. Irvine, A. J. McEvoy, M. Mogensen, S. C. Singhal, and J. Vohs, *Nat. Mater.*, **3**, 17 (2004).
4. Z. Zhan and S. A. Barnett, *Science*, **308**, 844 (2005).
5. S. Park, J. M. Vohs, and R. J. Gorte, *Nature*, **404**, 265 (2000).
6. J. Liu and S. A. Barnett, *Solid State Ionics*, **158**, 11 (2003).
7. E. N. Armstrong, J. Park, and N. Q. Minh, *Electrochem. Solid-State Lett.*, **15**, B75 (2012).
8. R. Muccillo, E. N. S. Muccillo, F. C. Fonseca, and D. Z. de Florio, *J. Electrochem. Soc.*, **155**, B232 (2008).
9. N. K. Monteiro, F. B. Noronha, L. O. O. Costa, M. Linardi, and F. C. Fonseca, *Int. J. Hydrogen Energy*, **37**, 9816 (2012).
10. G. A. Deluga, J. R. Salge, and X. E. Verykios, *Science*, **303**, 993 (2004).
11. S. L. Douvartzides, F. A. Coutelieris, A. K. Demin, and P. E. Tsiakaras, *Int. J. Hydrogen Energy*, **29**, 375 (2004).
12. Z. Zhan and S. C. Barnett, *Solid State Ionics*, **176**, 871 (2005).
13. X. F. Ye, S. R. Wang, Z. R. Wang, L. Xiong, X. F. Sun, and T. L. Wen, *J. Power Sources*, **177**, 419 (2008).
14. X. F. Ye, S. R. Wang, Q. Hu, Z. R. Wang, T. L. Wen, and Z. Y. Wen, *Electrochem. Commun.*, **11**, 823 (2009).
15. P. Vernoux, J. Guindet, and M. Kleitz, *J. Electrochem. Soc.*, **145**, 3487 (1998).
16. J. M. Klein, S. Georges, and Y. Bultel, *J. Appl. Electrochem.*, **40**, 943 (2010).
17. J. M. Klein, S. Georges, and Y. Bultel, *J. Electrochem. Soc.*, **155**, B333 (2008).
18. S. Georges, G. Parrour, M. Hénault, and J. Fouletier, *Solid State Ionics*, **177**, 2109 (2006).
19. J. M. Klein, M. Hénault, P. Gélin, Y. Bultel, and S. Georges, *Electrochem. Solid-State Lett.*, **11**, B144 (2008).
20. J. M. Klein, M. Hénault, C. Roux, Y. Bultel, and S. Georges, *J. Power Sources*, **193**, 331 (2009).
21. S. D. Nobrega, M. V. Galesco, K. Girona, D. Z. De Florio, M. C. Steil, S. Georges, and F. C. Fonseca, *J. Power Sources*, **213**, 156 (2012).
22. F. C. Fonseca, S. Uhlenbruck, R. Nedéléc, and H. P. Buchkremer, *J. Power Sources*, **195**, 1599 (2010).
23. M. Wisniewski, A. Boréave, and P. Gélin, *Catal. Commun.*, **6**, 596 (2005).
24. F. C. Fonseca and R. Muccillo, *Physica C*, **267**, 87 (1996).
25. V. Esposito, D. Z. de Florio, F. C. Fonseca, E. N. S. Muccillo, R. Muccillo, and E. Traversa, *J. Electrochem. Soc.*, **153**, A354 (2006).
26. J. Toyir, P. Gélin, H. Belatel, and A. Kaddouri, *Catal. Today*, **157**, 451 (2010).
27. G. Postole, K. Girona, J. Toyir, A. Kaddouri, and P. Gélin, *Fuel Cells*, **12**, 275 (2012).
28. L. V. Mattos, G. Jacobs, B. H. Davis, and F. B. Noronha, *Chem. Rev.*, **112**, 4094 (2012).
29. G. K. Gupta, A. M. Dean, K. Ahn, and R. J. Gorte, *J. Power Sources*, **158**, 497 (2006).
30. M. J.-F. Guinel and M. G. Norton, *J. Mater. Res.*, **21**, 2550 (2006).
31. B. Huang, X. Zhu, W. Hu, Y. Wang, and Q. Yu, *J. Power Sources*, **195**, 3053 (2010).
32. F. X. Ye, S. R. Wang, Q. Hu, J. Y. Chen, T. L. Wen, and Z. Y. Wen, *Solid State Ionics*, **180**, 276 (2009).
33. C. Mallon and K. Kendall, *J. Power Sources*, **145**, 154 (2005).
34. A. S. Ferlauto, D. Z. de Florio, F. C. Fonseca, V. Esposito, E. Traversa, R. Muccillo, and L. O. Ladeira, *Appl. Phys. A*, **84**, 271 (2006).